ACS OMEGA

Open Access

http://pubs.acs.org/journal/acsodf

Article

Investigations of a Copper(II) Bipyridyl-*N*-Heterocyclic Carbene Macrocycle for CO_2 Reduction: Apparent Formation of an Imidazolium Carboxylate Intermediate Leading to Demetalation

Sha Tamanna Sahil,[‖] Kaitlin M. McCardle,[‖] Pierre Le Magueres, Julien A. Panetier,* and Jonah W. Jurss*

Cite This: *ACS Omega* 2024, 9, 34555−34566

Read Online

ACCESS | Metrics & More | Article Recommendations | Supporting Information

ABSTRACT: A copper complex supported by a redox-active bipyridyl-*N*-heterocyclic carbene based ligand framework is reported. From X-ray crystallography, the tetradentate macrocycle provides a distorted square planar geometry around the copper metal center. The complex was investigated for the electrocatalytic CO_2 reduction reaction (CO_2RR) in acetonitrile solutions. Electronic structure calculations were performed on the complex and associated intermediates to provide a fundamental understanding of the metal−ligand redox chemistry and are compared to the previously reported nickel and cobalt analogues. Unlike its predecessors, which are active catalysts for the CO_2RR, the copper complex decomposes under reducing conditions in the presence of CO_2. A novel decomposition route involving coordination of CO_2 to an *N*-heterocyclic carbene (NHC) donor of the macrocyclic ligand is proposed based on density functional theory (DFT) calculations, which is supported by isolation of a putative ligand-CO_2 adduct from the electrolyzed solution and its characterization by ^{1}H NMR spectroscopy and mass spectrometry. The noninnocent behavior of the NHC donors presented here may have important implications for the stability and reactivity of other complexes supported by *N*-heterocyclic carbenes, and further suggests that cooperative and productive pathways involving metal-bound NHCs could be exploited for CO_2 reduction.

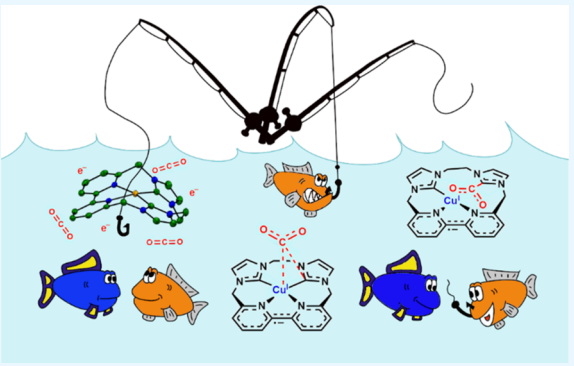

INTRODUCTION

Global energy consumption continues to rise, which remains strongly correlated with the accumulation of atmospheric greenhouse gas emissions due to our ongoing dependence on fossil fuels as an energy source. These trends are exacerbated by an increasing global population and an insatiable drive for economic growth.[1] Indeed, atmospheric CO_2 concentrations exceeded 415 ppm in 2018,[2] rising sharply since the Industrial Revolution from concentrations of less than 300 ppm during the previous 800,000 years.[3] Climate change and environmental catastrophes such as rising sea levels are expected if "business as usual" continues unabated.[4] Renewable energy sources offer sustainable alternatives to fossil fuels; however, these sources (i.e., solar and wind) are diffuse and provide irregular energy supplies that necessitate energy storage. In this context, renewable energy can drive the conversion of carbon dioxide into storable, energy-rich chemical fuels that are carbon neutral and compatible with existing infrastructure,[5] where CO_2 serves as an inexpensive chemical feedstock. However, more efficient catalysts are needed for this reaction. Catalyst design is critical in dictating product selectivity, turnover frequency, catalyst stability, and the energy input required to mediate the reaction.[5]

A growing number of transition metal catalysts for carbon dioxide reduction have been reported with ligands containing *N*-heterocyclic carbene (NHC) donors.[6−13] Electron-rich NHCs are good σ-donors that generally provide strong metal−ligand bonding interactions and improved catalyst durability, and their steric and electronic properties can be readily tuned to optimize catalytic performance.[14−17] We have recently developed a series of nickel- and cobalt-based catalysts featuring tunable tetradentate ligands (Scheme 1).[18,19] Structure−activity relationships were identified from both series in which the macrocyclic catalysts were found to be more active and selective than the non-macrocyclic systems (**1-M**) for CO_2 reduction in the presence of H_2O as a proton source, with the smallest macrocycles (**3-M**) performing best overall.[18,19] The nickel catalysts can generate methane in the

Received: March 18, 2024
Revised: July 12, 2024
Accepted: July 19, 2024
Published: July 31, 2024

Scheme 1. Previously Reported Nickel and Cobalt Catalysts for CO_2 Reduction Supported by Tunable Bipyridyl-*N*-heterocyclic Carbenes, M = Ni(II) or Co(II)

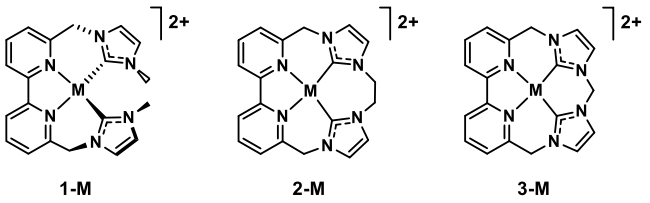

presence of a strongly reducing iridium photosensitizer and a sacrificial reductant. Catalyst **2-Ni** was found to be the most selective and active for this remarkable $8e^-/8H^+$ transformation.[20] Notably, lower overpotentials, faster turnover frequencies, and higher selectivities were obtained with the cobalt series in electrocatalytic CO_2 reduction. The cobalt catalysts can operate in aqueous solutions where **3-Co** generated CO with over 90% Faradaic efficiency.[19]

These catalysts exploit the bipyridyl unit as a redox-active fragment. Redox-active ligands can serve as effective electron reservoirs to facilitate the multielectron reduction of CO_2 but must work in concert with the metal for efficient catalysis.[18−28] However, in such systems, differences in reactivity as a function of metal are not well understood for molecular catalysts. Electronic structure calculations have shown, in the case of the nickel series (Scheme 1), that initial metal-based reductions favor proton reduction to H_2 while initial ligand-based reductions favor CO_2 reduction to CO.[18] A related observation was found for the cobalt series where initial ligand-based reductions gave improved selectivity for CO_2 conversion relative to the competing hydrogen evolution reaction (HER).[19] One of our primary objectives is to understand and exploit the interplay of metal−ligand redox chemistry in catalysts supported by redox-active frameworks. Our efforts were extended to copper to continue probing the synergy between the redox-active framework and an Earth-abundant metal center to understand how selectivity and activity for CO_2 reduction with added proton sources manifest as a function of the metal center. We report herein the synthesis, characterization, and electronic structure calculations of **2-Cu** (Scheme 2) supported by the 16-membered macrocycle (**L2**) featuring an ethyl bridge between the NHC donors.

Scheme 2. Synthesis of the Macrocyclic Copper Complex, 2-Cu, from the Imidazolium Ligand Precursor L2

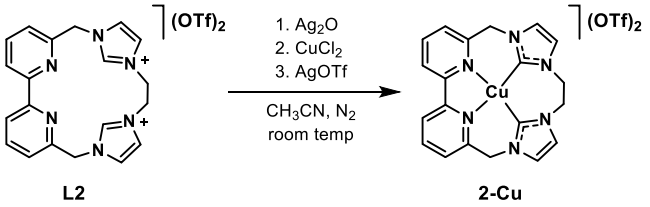

EXPERIMENTAL SECTION

Materials and Methods. All synthetic manipulations were performed under N_2 atmosphere using standard Schlenk techniques, unless otherwise noted. Acetonitrile was distilled over CaH_2 and stored over molecular sieves before use. Water was purified with a Barnstead NANOpure Diamond water purification system. All other chemicals were reagent or ACS grade, purchased from commercial vendors, and used without further purification. High-resolution electrospray ionization mass spectra (HR-ESI-MS) were acquired with a Waters SYNAPT HDMS Q-TOF mass spectrometer. ^{1}H NMR spectra were obtained using a Bruker Ascend 400 spectrometer operating at 400 MHz (^{1}H). Spectra were referenced to residual protiated solvent peaks, and chemical shifts are reported in ppm.

Electrochemical Measurements. Electrochemistry was performed with a CH Instruments 600E Series potentiostat. Cyclic voltammetry (CV) was carried out in a three-electrode cell equipped with a glassy carbon disk working electrode (3 mm dia.), a platinum wire counter electrode, and a silver wire quasi-reference electrode that was referenced at the end of experiments by the addition of ferrocene as an internal standard. Electrochemistry was conducted in acetonitrile (CH_3CN) solutions containing 0.1 M tetrabutylammonium hexafluorophosphate (Bu_4NPF_6) as the supporting electrolyte. Solutions for cyclic voltammetry were degassed with N_2 or CO_2 thoroughly before collecting data.

Controlled potential electrolysis (CPE) were performed in a 3-neck pear-shaped glass cell with a glassy carbon rod (2 mm diameter, type 2, Alfa Aesar) working electrode, a silver wire quasi-reference electrode, and a platinum mesh (2.5 cm^2 area, 150 mesh) counter electrode that was housed in an isolation chamber, separated from the other electrodes with a fine glass frit. Solutions were degassed with CO_2 for 30 min before collecting data. Applied potentials in CPE experiments were determined by cyclic voltammetry. Constant stirring was maintained during electrolysis. Headspace gases in the airtight vessel employed for electrolysis were quantified by gas chromatographic analysis using an Agilent 7890B Gas Chromatograph and an Agilent Porapak Q (6′ long, 1/8″ O.D.) column. Integrated gas peaks were quantified with calibration curves generated from known standards purchased from BuyCalGas.com. CO was measured at an FID detector equipped with a methanizer, while H_2 was quantified at the TCD detector. Faradaic efficiencies were determined from the experimental amount of product formed during electrolysis divided by the theoretical amount of product possible based on accumulated charge passed and the electron stoichiometry of the reaction × 100.

Ultraviolet−visible (UV−vis) spectroelectrochemical (SEC) measurements were conducted with a commercial "honeycomb" thin-layer SEC cell from Pine Research Instrumentation, employing a gold working electrode, a silver wire quasi-reference electrode, and a platinum wire counter electrode.

Synthetic Procedures. *Synthesis of L2(OTf)$_2$.* Compound **L2** was synthesized as the triflate salt of the imidazolium precursor according to a modified literature procedure.[18] In a 100 mL two-neck round-bottom flask, 6,6′-bis-(bromomethyl)−2,2′-bipyridyl (340 mg, 1.0 mmol) and 1-(2-(1*H*-imidazol-1-yl)ethyl)-1*H*-imidazole (162 mg, 1.0 mmol) were dissolved in 40 mL of a 1:1 (v/v) CH_3CN/H_2O solution and heated to reflux for 3 days while stirring under N_2 atmosphere. The solvent was then removed on a rotary evaporator and the remaining mass was dissolved in 30 mL of anhydrous CH_3CN. Silver triflate (514 mg, 2.0 mmol) was added to the reaction mixture, which was stirred overnight at room temperature under N_2 atmosphere. The reaction mixture was filtered through Celite to remove AgBr and the solvent was evaporated under reduced pressure. The compound was subsequently precipitated from an acetone

https://doi.org/10.1021/acsomega.4c02520
ACS Omega 2024, 9, 34555−34566

solution by adding diethyl ether and used without further purification (418 mg, 65%). ^{1}H NMR (400 MHz, CD_3CN): δ 8.61 (s, 2H), 7.97 (t, J = 7.8 Hz, 2H), 7.84 (d, J = 7.4 Hz, 2H), 7.55−7.52 (m, 4H), 7.46 (t, J = 1.9 Hz, 2H), 5.52 (s, 4H), 4.72 (s, 4H). ^{13}C NMR (400 MHz, CD_3CN): δ 157.17, 153.68, 139.33, 138.11, 125.29, 123.63, 123.32, 123.21, 54.34, 49.41.

*Synthesis of Cu(**L2**)(OTf)$_2$, **2-Cu**.* To a round-bottom flask was added 1.16 g (5 mmol) Ag_2O and 0.642 g (1 mmol) **L2**, which was dissolved in 30 mL dry acetonitrile and allowed to react at room temperature overnight under N_2 atmosphere. Excess Ag_2O was removed by centrifugation and filtration through a syringe filter (0.45 μm PTFE). Next, 0.134 g (1 mmol) $CuCl_2$ was added to the reaction mixture, which was stirred overnight at room temperature under an inert atmosphere. The reaction mixture was centrifuged and filtered through a syringe filter (0.45 μm PTFE) to remove AgCl. Next, 0.256 g (1 mmol) of AgOTf was added and stirred overnight at room temperature to remove the second equivalent of chloride. AgCl was again removed by centrifugation and filtration as described above. The product was purified by ether diffusion into a concentrated acetonitrile solution to afford purple crystals suitable for single-crystal X-ray diffraction (SCXRD). Yield = 27% (0.105 g). HR-ESI-MS (M^+) m/z calcd. for $[Cu(\mathbf{L2})]^{2+}$, 202.5445; found 202.5265. Elemental analysis calcd for $C_{22}H_{18}CuF_6N_6O_6S_2$: C, 37.53; H, 2.58; N, 11.94; found C, 37.35; H, 2.47; N: 11.76.

X-ray Crystallography. A single crystal of **2-Cu** was secured to a fiber loop micromount using Paratone oil and transferred to the goniometer head of a Rigaku XtaLAB Synergy-S X-ray diffractometer equipped with a HyPix-6000HE hybrid photon counting (HPC) detector, a micro-focused X-ray source, and an Oxford Cryosystems low-temperature device. Examination and data collection were performed with Mo Kα radiation (λ = 0.71073 Å) at 100 K. To ensure completeness and desired redundancy, data collection strategies were calculated using CrysAlisPro.[29] Subsequent data processing was also performed in CrysAlisPro. Using the SCALE3 ABSPACK scaling algorithm,[30] empirical absorption corrections determined via face-indexing in CrysAlisPro were applied to the data. The structure was solved via intrinsic phasing methods using ShelXT and refined using ShelXL in the Olex2 graphical user interface.[31−33] The final structural refinements included anisotropic temperature factors on all non-hydrogen atoms. All hydrogen atoms were placed according to their electron density Q-peak and refined as free atoms.

Additional data collection and refinement details can be found in Table S1. Complete crystallographic data, in CIF format, have been deposited with the Cambridge Crystallographic Data Centre. CCDC 2054810 contains the supplementary crystallographic data for this paper. These data can be obtained free of charge from The Cambridge Crystallographic Data Centre via www.ccdc.cam.ac.uk/data_request/cif.

Computational Details. Density functional theory (DFT) calculations were carried out with Gaussian 09 (Revision E.01),[34] and Gaussian 16 (Revision A.03).[35] Geometry optimizations were performed at the unrestricted ωB97X-D[36] level of theory in acetonitrile (ε = 35.688) through the solvation model based on density (SMD) approach.[37] The Def2-TZVPP basis set was used on Cu and Fe (i.e., ferrocene), while the Def2-SVP basis set was employed on all other atoms except for the triflate counteranion, in which Def2-SVPD was used (denoted BS1).[38,39] Additional single-point calculations were performed in solution on all optimized geometries using the Def2-TZVPP basis sets for all atoms except for the triflate in which Def2-TZVPPD was employed (denoted BS2). Stability analyses were performed in addition to analytical frequency calculations on all stationary points to ensure that geometries correspond to local minima (all positive eigenvalues) or transition states (one negative eigenvalue). IRC calculations and subsequent geometry optimizations were used to confirm the minima linked by each transition state.[40,41]

The oxidation state of the copper center was established through localized orbital bonding analysis (LOBA) calculations on the ωB97X-D/BS1(SMD) optimized geometries,[42] as implemented in the Q-Chem software.[43] The Pipek−Mezey orbitals were utilized in combination with the Löwdin population analysis. All computed free energies include the zero-point vibrational energy corrections, thermal corrections, and entropies calculated by standard statistical thermodynamic methods at 298.15 K and 1 M standard state. The computed Gibbs free energies were corrected by implementing Grimme's quasi-harmonic approach to entropic contributions and Head-Gordon's quasi-harmonic approach to enthalpy.[44,45] All calculated reduction potentials are reported versus the $Fc^{+/0}$ couple and were computed using the direct method.[46] Unless otherwise stated, all reported free energies were obtained at the ωB97X-D/BS2(SMD)//ωB97X-D/BS1(SMD) level of theory. Additional benchmarking calculations were performed using generalized gradient approximation (GGA), Hybrid GGA, and meta hybrid-GGA functionals. Further details are provided in the Supporting Information.

RESULTS

The macrocyclic copper complex (**2-Cu**) was synthesized from the bipyridyl-imidazolium ligand precursor (**L2**) as summarized in Scheme 2. An intermediate silver-NHC complex was formed by reacting **L2** with excess Ag_2O, which was subsequently transmetalated with $CuCl_2$ to form a copper complex and one equivalent of AgCl. The copper species was reacted with one equivalent of AgOTf to remove the second chloride ion to give the triflate salt of **2-Cu**, which was purified by diethyl ether diffusion into a concentrated acetonitrile solution to afford purple crystals suitable for single-crystal X-ray diffraction.

The X-ray crystal structure of **2-Cu** exhibits a distorted square planar geometry in which the copper metal center is coordinated to the two nitrogen atoms from the bipyridine moiety and a carbon atom from each NHC donor (Figure 1). The bond distances from the Cu center to the two nitrogens of bipyridine are 2.0619(13) and 2.0592(15) Å, and from the Cu center to the two carbons of the NHC donors, 1.9835(18) and 1.9980(16) Å. The crystal structure also reveals a specific association of two triflate ions with the axial coordination sites of the copper species with Cu−O distances of 2.6557(12) and 2.8145(12) Å. The Cu−O distances are significantly longer (by 0.5−0.8 Å) than the sum of the covalent radii of Cu and O, but between 0.1 and 0.3 Å shorter than the sum of their van der Waals radii, consistent with an electrostatic interaction between the copper cation and the triflate counteranions.[47,48] Thus, we favor a four-coordinate description of the copper complex, in agreement with the computational results (*vide infra*).

The 16-membered macrocycle has a moderate degree of flexibility. The chelate angles around the copper center vary from 78.21(6)° for the N1−Cu−N2 angle formed by the

https://doi.org/10.1021/acsomega.4c02520
ACS Omega 2024, 9, 34555−34566

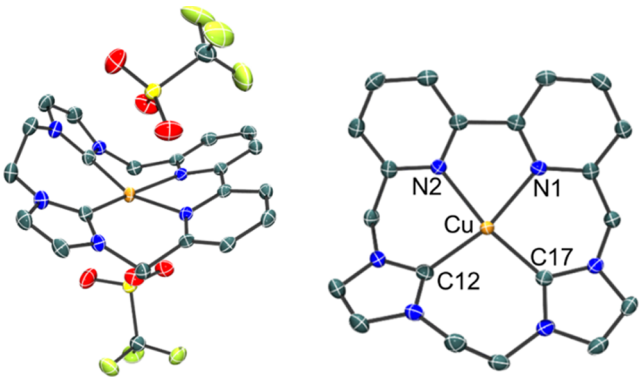

Figure 1. ORTEP diagrams of **2-Cu** with (left) and without (right) the associated triflate ions. Thermal ellipsoids are shown at 70% probability. H atoms and an outer sphere acetonitrile molecule have been omitted for clarity.

bipyridine donor as part of a 5-membered chelate ring to 100.43(7)° for the C12−Cu−C17 angle comprised of the NHC donors as part of a 7-membered chelate ring. Intermediate to these extremes, the N1−Cu−C17 and N2−Cu−C12 angles dictated by the opposing 6-membered chelate rings are 91.06(6) and 88.62(6)°, respectively. The bipyridine unit is nearly planar and exhibits a torsion angle between the pyridine rings of just 0.22°.

Electrochemistry. The electrochemical behavior of the complex was examined by cyclic voltammetry in N_2-saturated solutions containing 1 mM **2-Cu** with 0.1 M Bu_4NPF_6 as the supporting electrolyte in anhydrous acetonitrile (CH_3CN). All potentials are referenced to the ferrocenium/ferrocene couple ($Fc^{+/0}$). The potential was scanned negatively where an irreversible peak is observed at −0.89 V, which is followed by a reversible redox couple at $E_{1/2}$ = −2.10 V with a peak splitting value of 69 mV (Figure 2). Continuing with the return

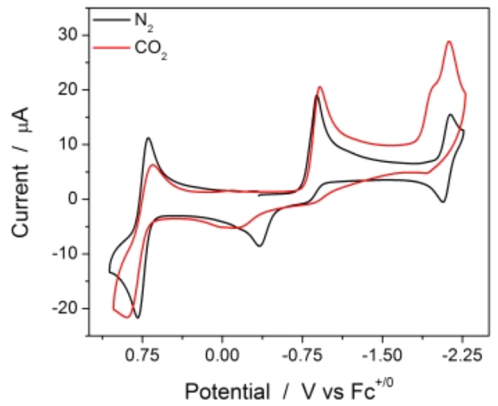

Figure 2. Cyclic voltammetry of **2-Cu** at 1 mM concentration in anhydrous CH_3CN/0.1 M Bu_4NPF_6 solutions under N_2 (black) and CO_2 (red) atmosphere at a scan rate of 100 mV/s.

scan, a peak at −0.35 V is observed, along with a quasi-reversible couple at $E_{1/2}$ = 0.74 V (ΔE = 99 mV). The most positive redox process is assigned to a Cu(III/II) couple, while the waves at −0.89 and −2.10 V are tentatively assigned to Cu(II/I) and ligand-based reductions, respectively. Cyclic voltammograms were collected as a function of scan rate. The reductive peak potentials were found to exhibit linear behavior when plotted versus the square root of the scan rate, consistent with diffusion-controlled processes (Figure S1).

The same solution was then examined under a CO_2 atmosphere. Under these conditions, a small increase in current and a slight cathodic shift are observed for the first reduction, relative to that under N_2, at −0.92 V. At more negative potentials, two overlapping and predominately irreversible reductions are observed at −1.95 and −2.12 V that constitute a relatively significant increase in current in the presence of CO_2. These results are consistent with CO_2 activation by the reduced complex. In the return scan, broad oxidation features appear at −0.89 and −0.12 V, followed by a prominent oxidation wave at 0.89 V. The putative Cu(III/II) couple is also less reversible. Scan rate dependent cyclic voltammograms reveal that the system remains diffusion-controlled under these conditions (Figure S3).

Controlled potential electrolysis (CPE) was carried out at an applied potential of −2.14 V using a high surface area glassy carbon rod working electrode to determine the stability and selectivity of **2-Cu** for electrocatalytic CO_2 reduction (Figure 3A). During the CPE experiment, the solution changes from a homogeneous light pink solution to an off-white and turbid solution (Figure S4). This apparent degradation is noticeable within the first 30 min of the experiment. The electrolyzed solution was filtered and examined by high-resolution mass spectrometry and ^{1}H NMR spectroscopy. In the mass spectrum, there was no signal corresponding to the metal complex, but peaks matching the m/z ratio and isotopic pattern of the free ligand bearing a CO_2 adduct were observed (Figure S5). A ^{1}H NMR spectrum was also obtained that supports the mass spectrometry data; the proposed structure is shown in Figure 4. It was challenging to isolate the compound from the supporting electrolyte (0.1 M Bu_4NPF_6) and only a small amount was collected, which prevented further characterization. In the ^{1}H NMR spectrum, 10 aromatic protons are observed between 7.3 and 8.6 ppm that we assign to the aromatic protons of the bipyridine and the protons at the 4 and 5 positions of the imidazolium groups of an asymmetric compound. Additional signals are found between 3.9 and 5.6 ppm that integrate to a total of 8 protons that presumably correspond to the alkyl linking groups within the macrocycle. However, we are not able to explain the integrations of ∼3 for the peaks at 3.98 and 4.44 ppm based on the proposed structure. Further downfield, a singlet that integrates to 1 is observed at 10.09 ppm that is assigned to an imidazolium C2 proton, which may have a hydrogen-bonding interaction with the carboxylate given its chemical shift. At a minimum, these results indicate that the complex demetalates under reducing conditions. Indeed, the glassy carbon rod was coated with a thin metallic layer, consistent with the deposition of a heterogeneous Cu material on the electrode surface (Figure S4). The used electrode was then subjected to a rinse test and was found to exhibit a catalytic current response in a fresh, catalyst-free solution of electrolyte saturated with CO_2 (Figure 3B). Metallic copper is a known heterogeneous catalyst for electrochemical CO_2 to a variety of reduced carbon products.[49−53]

An electrolysis with **2-Cu** at an applied potential of −0.96 V, just after the first reduction, was also conducted and produced the same product. The putative ligand-CO_2 adduct was again identified by ^{1}H NMR spectroscopy as a component of the mixture following this experiment (Figure S6). Under anhydrous conditions, protonation of the C2 carbon of one of the NHC donors to form an imidazolium moiety is expected to come from Hofmann degradation of the quaternary

https://doi.org/10.1021/acsomega.4c02520
ACS Omega 2024, 9, 34555−34566

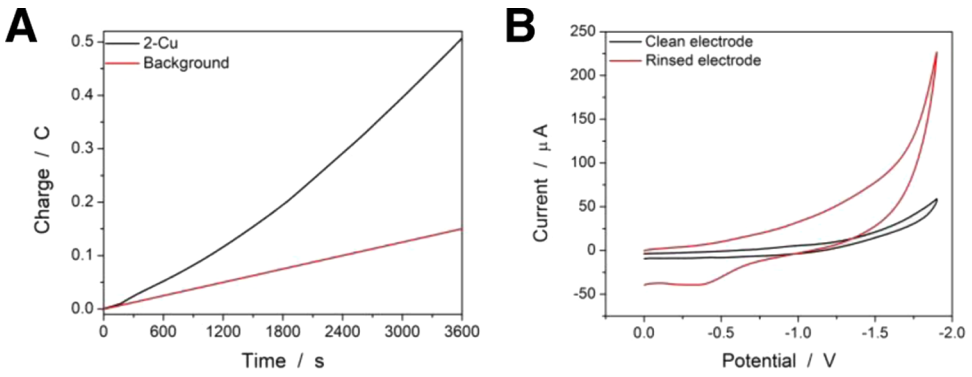

Figure 3. Charge-time profile from CPE experiments with 0.5 mM of **2-Cu** in CO_2-saturated CH_3CN/0.1 M Bu_4NPF_6 solution at −2.14 V vs $Fc^{+/0}$ (A); CVs associated with the rinse test using fresh electrolyte solution, ν = 100 mV/s (B).

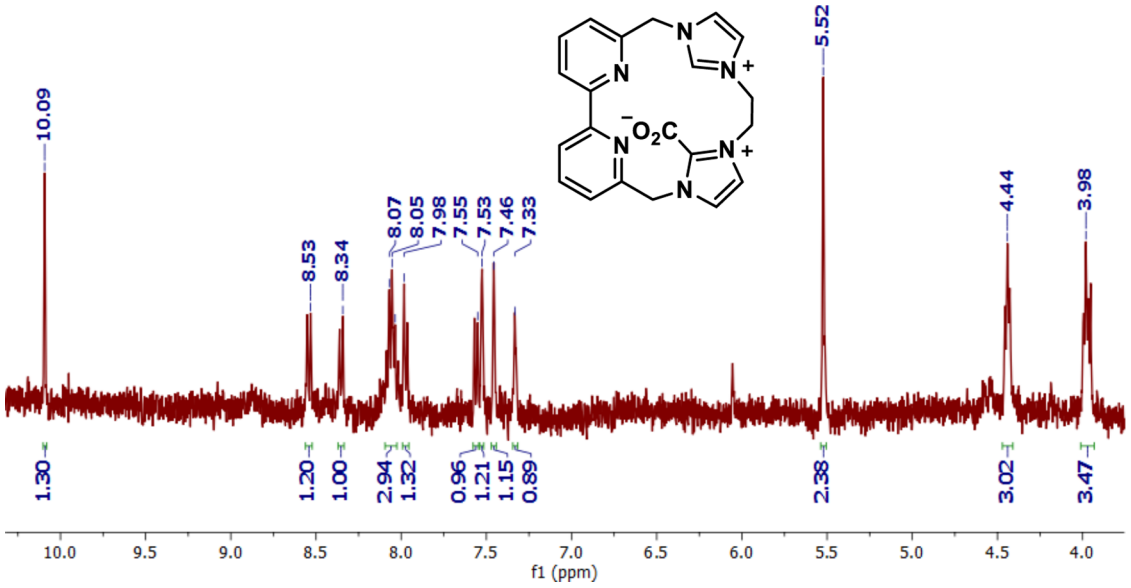

Figure 4. ^{1}H NMR spectrum of the isolated ligand-CO_2 adduct in CD_3CN. The proposed structure is shown.

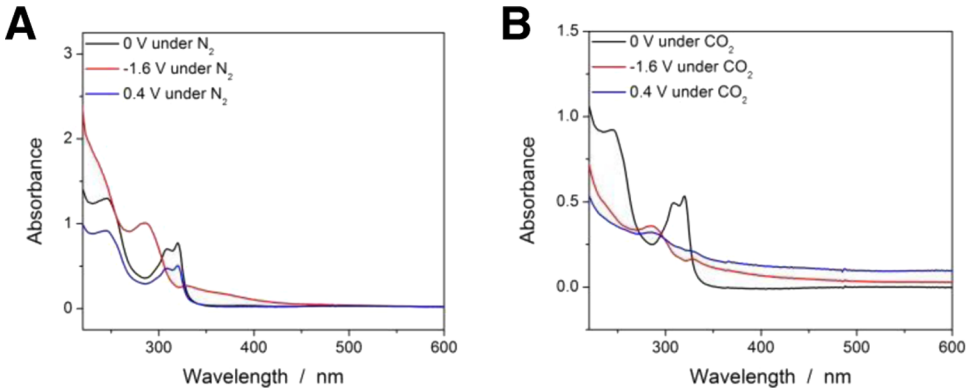

Figure 5. UV−vis spectroelectrochemistry of 0.125 mM **2-Cu** in N_2- (A) and CO_2- (B) saturated anhydrous CH_3CN/0.1 M Bu_4NPF_6 solutions.

alkylammonium cation of the supporting electrolyte, which is well-established under reducing conditions.[54,55]

It is known that *N*-heterocyclic carbenes can be generated electrochemically from imidazolium salts[56−62] and reacted with various electrophiles,[58−62] including CO_2.[60] We reasoned that it would be possible to generate a free carbene from ligand precursor **L2** under reducing conditions, which could react with CO_2 in the absence of a copper ion. To test this possibility, an electrolysis of **L2** was performed at the same applied potential (−0.96 V) in CO_2-saturated CH_3CN/0.1 M Bu_4NPF_6 (Figure S7). However, the adduct was not observed by ^{1}H NMR spectroscopy under these conditions (Figure S8), indicating that the Cu metal center plays an important role in the formation of the proposed ligand-CO_2 decomposition product.

The electrochemical activity and stability of **2-Cu** was also investigated in the presence of water as an added proton source to facilitate the proton-coupled reduction of CO_2. Current

https://doi.org/10.1021/acsomega.4c02520
ACS Omega 2024, 9, 34555−34566

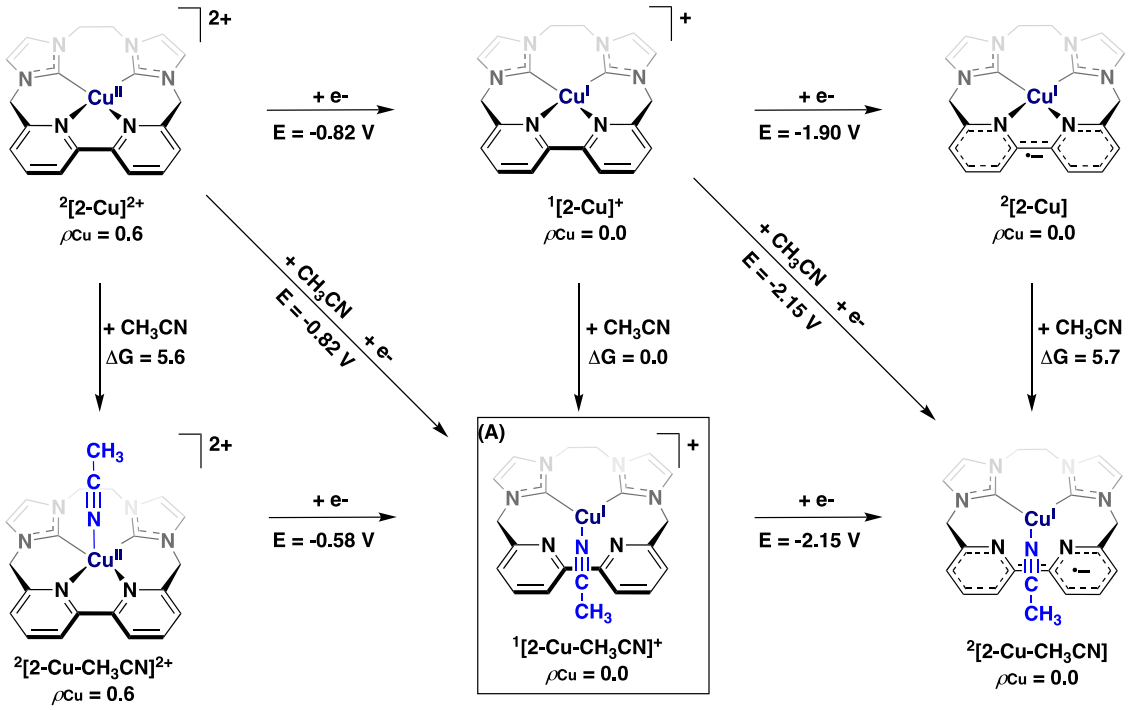

Figure 6. Calculated redox potentials in V versus the $Fc^{+/0}$ couple for the one- and two-electron reduced species from ^{2}[**2-Cu**]$^{2+}$ in acetonitrile. The Mulliken spin population is given for copper, ρ_{Cu}. (A) Proposed distorted trigonal planar intermediate, ^{1}[**2-Cu-CH$_3$CN**]$^+$, obtained after the first reduction. The computed free energy profile leading to the formation of this intermediate is shown in Figure 7.

enhancement was observed in cyclic voltammograms with increasing concentrations of added water until saturation conditions were achieved at concentrations of 2.4% (v/v) added H_2O (Figure S9). A controlled potential electrolysis of **2-Cu** in CO_2-saturated CH_3CN solution containing 2.4% H_2O was then performed with an applied potential of −2.14 V (Figure S10). An overall Faradaic efficiency (FE) of 15% (FE_{CO} = 12%; FE_{H2} = 3%) was determined by analyzing the headspace gases of the airtight electrochemical cell by gas chromatography. The post-CPE solution was also analyzed and a small amount of the ligand-CO_2 adduct was observed by ^{1}H NMR spectroscopy (Figure S11). However, under these conditions with added water, the major decomposition product observed by ^{1}H NMR is a species in which both NHC donors are protonated, indicating that protonation of the NHCs significantly outcompetes CO_2 binding.

UV−Visible Spectroelectrochemistry. Prompted by the CPE experimental results, UV−vis spectroelectrochemistry was performed at different applied potentials under both N_2 and CO_2 atmospheres. The UV−vis spectrum of **2-Cu** has an absorption band at 320 nm that is accompanied by a shoulder at 309 nm and another peak at 244 nm. With an applied potential of −1.60 V, beyond the first reduction, a new peak appears at 285 nm along with a small absorption at 330 nm that features a tailing band out to ∼450 nm; these peaks emerge at the expense of the initial spectrum (Figure 5A). The reversibility of this process was assessed with an applied potential of 0.4 V to oxidize the complex back to the starting Cu(II) state. The resulting spectrum is less intense but is otherwise identical to the initial spectrum. The same experiment was conducted under CO_2 atmosphere using a fresh solution of **2-Cu**. However, in the presence of CO_2, an irreversible change in the absorption spectrum is observed, and regeneration of the initial complex was not achieved (Figure 5B). A rise in the baseline absorbance is observed at longer wavelengths that is indicative of light scattering and the formation of a turbid solution. This behavior suggests that the reaction of CO_2 with the reduced complex facilitates decomposition.

Computational Results. Density functional theory (DFT) calculations were performed for the four-coordinate [**2-Cu**]$^{2+}$ complex and its one- and two-electron reduced species. Starting with ^{2}[**2-Cu**]$^{2+}$ (where the initial superscript represents the spin multiplicity of a species, in this case, doublet), the four-coordinate complex was computed to have a dihedral angle (τ) between the two ligand planes (Cu−C_2 and Cu−N_2) that deviates from the ideal square planar geometry by 13.7° (exp. τ = 16.55(6)°). This deviation is slightly higher than in the cobalt and nickel counterparts, which have calculated deviations of 10.2° and 9.2° (exp. τ = 6.40(9)° for **2-Ni**), respectively. This indicates that the copper compound is somewhat more distorted and may behave differently than its nickel and cobalt analogs. We note that the higher degree of distortion of the ligand framework is also observed experimentally, where τ = 16.55(6)° for **2-Cu**. The computed bond lengths are in good agreement with the experimental values. For instance, the Cu−N bond distances are calculated as 2.090 and 2.103 Å (vs 2.0619 and 2.0592 Å experimentally). In comparison, the Cu−C bond distances associated with the NHC donors are computed as 1.996 and 2.016 Å compared to 1.9835 and 1.9980 Å experimentally. Localized orbital bonding analysis (LOBA) calculations were performed on the ^{2}[**2-Cu**]$^{2+}$ species and confirmed that the copper metal center is formally in a +2 oxidation state (Figure S19). We have also considered five- and six-coordinate compounds in the presence of acetonitrile. However, an octahedral compound could not be formed as one of the bound acetonitriles would dissociate and weakly interact with the metal center. In the case of the

https://doi.org/10.1021/acsomega.4c02520
ACS Omega 2024, 9, 34555−34566

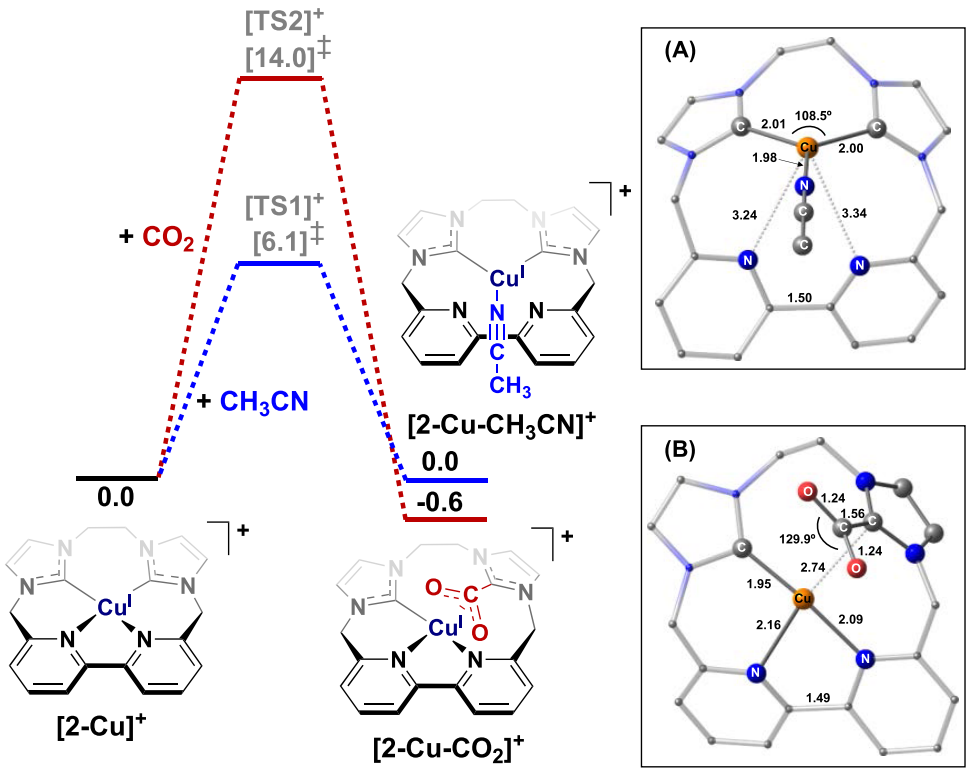

Figure 7. Computed free energy (kcal/mol) profiles for yielding the acetonitrile bound species, [**2-Cu-CH$_3$CN**]$^+$, and CO_2 adduct intermediate, [**2-Cu-CO$_2$**]$^+$, in which carbon dioxide binds at the NHC donor. All free energies are calculated with respect to the separated reactants, and all species have a singlet ground state. (A) Optimized geometry of the three-coordinate acetonitrile bound complex, [**2-Cu-CH$_3$CN**]$^+$. (B) Optimized geometry of [**2-Cu-CO$_2$**]$^+$ in which CO_2 is bound to the NHC donor. The distances are in Å, and the angles are in degrees.

five-coordinate species, our calculations suggest that acetonitrile binding to yield ^{2}[**2-Cu-CH$_3$CN**]$^{2+}$ is uphill by 5.6 kcal/mol and is, therefore, unlikely under the experimental conditions (Figure 6). Similar observations were obtained in the presence of triflate (Figure S18). Our computational results are consistent with a four-coordinate description of the copper complex [**2-Cu**]$^{2+}$.

The first redox potential was obtained by optimizing the four-coordinate [**2-Cu**]$^{2+}$ complex and its one-electron-reduced species in acetonitrile. The calculated redox potential from the four-coordinate copper(II) compound to the one-electron reduced species is within 70 mV of the experimental value (Figure 6). Note that various tested DFT functionals show similar results (Table S7). The reduction is metal-centered and yields a four-coordinate closed-shell singlet, ^{1}[**2-Cu**]$^+$. LOBA calculations confirm that the oxidation state of copper is +1 (Figure S24). The formal oxidation state of +1 for ^{1}[**2-Cu**]$^+$ differs from the nickel and cobalt analogs, where both the ligand and metal-based reductions are accessible in **2-Ni**.[18] In contrast, the initial reduction of **2-Co** is ligand-centered.[19] These observations are explained by the higher degree of distortion of the ligand framework in **2-Cu**, which stabilizes the $d_{x^2-y^2}$ orbital with respect to the bpy π^* orbital compared to the nickel and cobalt analogues, as shown for the one-electron reduced species (Figure S31).

A critical aspect of our work is that following the formation of ^{1}[**2-Cu**]$^+$, acetonitrile can bind at copper to give a three-coordinate ^{1}[**2-Cu-CH$_3$CN**]$^+$ species, where the bipyridine ligand dissociates (Cu···N$_{py}$ = 3.24 Å and Cu···N$_{py}$ = 3.34 Å, Figure 7A) upon CH_3CN binding. This intermediate is at equilibrium with the separated reactants (Figures 6 and 7). A transition state was located for this process, which requires an activation energy of 6.1 kcal/mol, implying that the formation of the proposed distorted trigonal planar complex is kinetically and thermodynamically accessible. Since ^{1}[**2-Cu-CH$_3$CN**]$^+$ is at equilibrium with the separated reactants, acetonitrile binding and reduction of ^{2}[**2-Cu**]$^{2+}$ via a concerted process displays the same redox potential as the stepwise pathway. This suggests both mechanisms are viable experimentally, which may explain the irreversible peak observed at −0.89 V.

In the second redox event, the four-coordinate species ^{1}[**2-Cu**]$^+$ can be reduced to form ^{2}[**2-Cu**]^0 at −1.90 V, which is 200 mV more positive than the experimental value ($E_{1/2}$ (exp.) = −2.10 V, $E_{1/2}$ (calc.) = −1.90 V; Table S8). However, an alternative mechanism provides a better agreement between the theoretical and experimental redox potentials. After the first reduction event, a distorted trigonal planar complex, ^{1}[**2-Cu-CH$_3$CN**]$^+$, can form, as previously described, which can be reduced to give ^{2}[**2-Cu-CH$_3$CN**], the corresponding three-coordinate neutral species (Figure 6). In this case, the computed redox potential is −2.15 V, which agrees with the experimental value ($E_{1/2}$ = −2.10 V). Moreover, the reduction is ligand-based to yield a copper(I) center and a bipyridine π^* radical.

In addition to acetonitrile coordination, CO_2 binding was also considered after the initial formation of ^{1}[**2-Cu**]$^+$. In light of the observed geometry of the acetonitrile-bound species, we considered CO_2 binding to the copper center with three-, four-, and five-coordinate geometries, as well as CO_2 binding to the carbon atom of one of the NHC ligands. While we could not obtain a metallocarboxylate intermediate species on the singlet surface, our calculations imply that CO_2 binding to the

https://doi.org/10.1021/acsomega.4c02520
ACS Omega 2024, 9, 34555−34566

NHC ligand is spontaneous by 0.6 kcal/mol, signifying that the primary interaction of CO_2 with the catalyst takes place at the *N*-heterocyclic carbene. A transition state was located to give the ligand-coordinated CO_2 adduct, ^{1}[**2-Cu-CO$_2$**], which has a free energy of activation of 14.0 kcal/mol that may be due, in part, to the structural rearrangement that occurs during the breaking of the Cu-NHC bond. Experimentally, there is evidence of CO_2 bound to the free ligand (Figure S5), suggesting that catalyst deactivation may occur due to CO_2 binding to the NHC donor rather than at the copper metal center. We have also computationally considered direct CO_2 binding at the free imidazolium ligand. Further details are provided in the Supporting Information.

DISCUSSION

The catalytic reduction of carbon dioxide using molecular copper complexes is rare.[63−66] This is likely due to the limited stability that is often observed under reducing conditions. Indeed, the reductive demetalation of molecular copper complexes has been reported with various ligand frameworks, including macrocycles.[67−74] It has been shown previously that demetalation by electrochemical reduction results in the deposition of metallic copper on the electrode surface.[66,72] Farnum and co-workers demonstrated that the deposited copper layer was a competent electrocatalyst for CO_2-to-CO conversion.[66] As heterogeneous electrocatalysis is not the focal point of this work, additional studies beyond the rinse test described above (Figure 3B) were not pursued here.

Experimental and computational data indicate that the large peak-to-peak splitting of the Cu(II/I) couple at −0.89 V corresponds to the reduction of copper and subsequent formation of a distorted trigonal planar intermediate in acetonitrile (Figure 6). This complex is at equilibrium with the separated reactants and requires an activation energy of 6.1 kcal/mol (Figure 7), which is kinetically and thermodynamically accessible under experimental conditions. Furthermore, TD-DFT calculations of ^{1}[**2-Cu-CH$_3$CN**]$^+$ indicate that the UV−vis spectrum reasonably agrees with the experimental data (Figures 5 and S34). However, the theoretical spectrum computed for ^{1}[**2-Cu**]$^+$ also matches the experimental UV−vis data, implying that both ^{1}[**2-Cu**]$^+$ and ^{1}[**2-Cu-CH$_3$CN**]$^+$ are at equilibrium, as described previously.

It is worth noting that a number of three-coordinate Cu(I) compounds supported by carbene-based ligands are known in the literature.[75−78] In these examples, trigonal planar geometries are typically observed with either one or two coordinated NHC donors.[75−77] Relevant examples of copper complexes in different oxidation states bearing macrocyclic tetradentate NHC based ligands have also been reported.[79,80] In the report by Kühn and co-workers using a tetraNHC ligand, a Cu(III) complex was accessed via a disproportionation reaction starting from a Cu(II) salt even under anaerobic conditions.[79] Interestingly, the copper(III) metal center can react with acetate to cause decoordination of the macrocycle along with oxidation of an NHC donor.[79] In the report by Meyer and co-workers, the stepwise preparation and isolation of copper complexes in the +1, +2, and +3 oxidation states was shown with a dipyridyl-diNHC ligand in which the two NHCs of the macrocycle are positioned *trans* to one another (rather than *cis* as in **2-Cu**).[80] Our efforts to isolate and characterize a Cu(I) species from **L2** or by reduction of **2-Cu** were not successful. We reason that the *trans* orientation of NHC groups in the Meyer system[80] is an important characteristic, facilitating the isolation of a stable Cu(I) complex as most Cu(I)-NHC compounds adopt a linear geometry with many displaying a cationic $[Cu(I)(NHC)_2]^+$ motif.[79]

Our work also demonstrates that CO_2 binds at the NHC ligand rather than at copper. For instance, DFT calculations indicate that after forming ^{1}[**2-Cu**]$^+$, ^{1}[**2-Cu-CO$_2$**]$^+$ is exergonic by 0.6 kcal/mol (Figure 7). Moreover, the computed UV−vis spectrum for this compound matches the experimental data (Figures 5 and S35). Also, based on our calculations, ^{1}[**2-Cu-CO$_2$**]$^+$ is proposed to be the thermodynamic product, while ^{1}[**2-Cu-CH$_3$CN**]$^+$ is the kinetic product when both CH_3CN and CO_2 are present in solution (Figure 7). The formation of a ligand-coordinated CO_2 adduct intermediate becomes even more favorable after adding one additional electron to ^{1}[**2-Cu**]$^+$ to give ^{2}[**2-Cu**], where the latter compound features a copper(I) center and a bipyridine π^* radical. In this case, the formation of ^{2}[**2-Cu-CO$_2$**] is spontaneous (ΔG = −4.6 kcal/mol) and requires an activation energy of 11.9 kcal/mol (Figure S30). This is consistent with the experimental CV of **2-Cu** under a CO_2 atmosphere, which displays an increase in current and a slight cathodic shift of the two overlapping and predominately irreversible reductions at −1.95 and −2.12 V. The isolation of an apparent ligand-CO_2 adduct in the post-electrolysis solution falls in line with the theoretical outcome. Moreover, this same adduct is also observed following electrolysis with an applied potential corresponding to the first reduction potential.

N-heterocyclic carbene-based ligands have been widely applied in homogeneous catalysis, including electrocatalytic CO_2 reduction with first-row transition metals,[7−11,18−20] as neutral, highly tunable donors that provide robust metal−ligand bonding interactions.[14−17] However, NHCs are also electron-rich nucleophiles that have been shown to react reversibly with CO_2 to form neutral zwitterionic imidazolium carboxylates.[81−84] We note that NHC−CO_2 adducts can be prepared by other routes,[85−87] and such compounds have been used to convert CO_2 into methanol and methane.[88,89] Interestingly, imidazolium carboxylates have been employed as NHC-transfer agents to form metal-carbene complexes while releasing CO_2,[84,90,91] which may be considered the reverse reaction of the demetalation pathway proposed here to form the ligand-derived NHC−CO_2 adduct.

CONCLUSIONS

A new copper complex featuring a tetradentate bipyridyl-NHC based ligand was prepared. This 16-membered macrocyclic compound was characterized by elemental analysis, high-resolution mass spectrometry, and X-ray crystallography. As part of a larger series of compounds, the copper complex was investigated for electrocatalytic CO_2 reduction, but was found to be unstable under these conditions.

DFT calculations were pursued to provide a fundamental understanding of the electronic structures of **2-Cu** and associated intermediates with respect to its nickel and cobalt analogues. Due to the higher deviation from the ideal square planar geometry in **2-Cu**, the $d_{x^2-y^2}$ orbital is more stabilized than in **2-Ni** and **2-Co**. A direct consequence of this is that the metal is mainly reduced in going from ^{2}[**2-Cu**]$^{2+}$ to ^{1}[**2-Cu**]$^+$, while a ligand-based reduction is accessible in both the nickel and cobalt derivatives.[18,19] We note that in the case of **2-Ni**, the metal-based reduction was also computed to be competitive.[18]

https://doi.org/10.1021/acsomega.4c02520
ACS Omega 2024, 9, 34555−34566

A novel decomposition pathway is proposed based on electronic structure calculations reported here, in which carbon dioxide binds to an NHC donor of the ligand and ultimately leads to demetalation of the ligand. Data obtained by ^{1}H NMR spectroscopy and high-resolution mass spectrometry following controlled potential electrolysis of the copper complex in CO_2-saturated acetonitrile solutions suggest that the free ligand bearing a CO_2-adduct is formed. The proposed pathway for catalyst decomposition has not been previously reported, to the best of our knowledge, and may be relevant to the growing number of NHC-based catalysts employed for CO_2 reduction. Furthermore, the noninnocent behavior of the NHC donors proposed here suggests that cooperative and productive pathways involving metal-bound NHCs could be exploited for CO_2 reduction catalysis.

■ ASSOCIATED CONTENT

Supporting Information

The Supporting Information is available free of charge at https://pubs.acs.org/doi/10.1021/acsomega.4c02520.

Crystal data and refinement details, electrochemical data, characterization of products after electrolysis, computational data, references, Cartesian coordinates and computed energies (PDF)

2Cu_b_bigger_Mo_Manual (CIF)

■ AUTHOR INFORMATION

Corresponding Authors

Julien A. Panetier − *Department of Chemistry, State University of New York at Binghamton, Binghamton, New York 13902, United States;* orcid.org/0000-0003-4905-8396; Email: panetier@binghamton.edu

Jonah W. Jurss − *Department of Chemistry and Biochemistry, University of Mississippi, University, Mississippi 38677, United States;* orcid.org/0000-0002-2780-3415; Email: jwjurss@olemiss.edu

Authors

Sha Tamanna Sahil − *Department of Chemistry and Biochemistry, University of Mississippi, University, Mississippi 38677, United States*

Kaitlin M. McCardle − *Department of Chemistry, State University of New York at Binghamton, Binghamton, New York 13902, United States;* orcid.org/0000-0002-8464-1416

Pierre Le Magueres − *Rigaku Americas Corporation, The Woodlands, Texas 77381, United States*

Complete contact information is available at: https://pubs.acs.org/10.1021/acsomega.4c02520

Author Contributions

‖S.T.S. and K.M.M. contributed equally to this work.

Notes

The authors declare no competing financial interest.

■ ACKNOWLEDGMENTS

S.T.S. and J.W.J. thank the National Science Foundation for generous support through a CAREER Award CHE-1848478. This research was also supported by the National Institute of General Medical Sciences of the National Institutes of Health under Award Number R15GM131290. The content is solely the responsibility of the authors and does not necessarily represent the official views of the National Institutes of Health. Electronic structure calculations were performed on the Spiedie cluster at Binghamton University and the Extreme Science and Engineering Discovery Environment (XSEDE), supported by the National Science Foundation grant number ACI-1548562, under allocation TG-CHE180009.

■ REFERENCES

(1) Mardani, A.; Streimikiene, D.; Cavallaro, F.; Loganathan, N.; Khoshnoudi, M. Carbon Dioxide (CO_2) Emissions and Economic Growth: A Systematic Review of Two Decades of Research from 1995 to 2017. *Sci. Total Environ.* **2019**, *649*, 31−49.

(2) Hashimoto, K. Global Temperature and Atmospheric Carbon Dioxide Concentration. In *Global Carbon Dioxide Recycling*; Springer: Singapore, 2019.

(3) Lüthi, D.; Le Floch, M.; Bereiter, B.; Blunier, T.; Barnola, J.-M.; Siegenthaler, U.; Raynaud, D.; Jouzel, J.; Fischer, H.; Kawamura, K.; Stocker, T. F. High-Resolution Carbon Dioxide Concentration Record 650,000−800,000 Years Before Present. *Nature* **2008**, *453*, 379−382.

(4) Lewis, N. S.; Nocera, D. G. Powering the Planet: Chemical Challenges in Solar Energy Utilization. *Proc. Natl. Acad. Sci. U.S.A.* **2006**, *103*, 15729−15735.

(5) (a) Benson, E. E.; Kubiak, C. P.; Sathrum, A. J.; Smieja, J. M. Electrocatalytic and Homogeneous Approaches to Conversion of CO_2 to Liquid Fuels. *Chem. Soc. Rev.* **2009**, *38*, 89−99. (b) Yui, T.; Tamaki, Y.; Sekizawa, K.; Ishitani, O. Photocatalytic Reduction of CO_2: From Molecules to Semiconductors. *Top. Curr. Chem.* **2011**, *303*, 151−184. (c) Finn, C.; Schnittger, S.; Yellowlees, L. J.; Love, J. B. Molecular Approaches to the Electrochemical Reduction of Carbon Dioxide. *Chem. Commun.* **2012**, *48*, 1392−1399. (d) Appel, A. M.; Bercaw, J. E.; Bocarsly, A. B.; Dobbek, H.; DuBois, D. L.; Dupuis, M.; Ferry, J. G.; Fujita, E.; Hille, R.; Kenis, P. J. A.; Kerfeld, C. A.; Morris, R. H.; Peden, C. H. F.; Portis, A. R.; Ragsdale, S. W.; Rauchfuss, T. B.; Reek, J. N. H.; Seefeldt, L. C.; Thauer, R. K.; Waldrop, G. L. Frontiers, Opportunities, and Challenges in Biochemical and Chemical Catalysis of CO_2 Fixation. *Chem. Rev.* **2013**, *113*, 6621−6658. (e) Kang, P.; Chen, Z.; Brookhart, M.; Meyer, T. J. Electrocatalytic Reduction of Carbon Dioxide: Let the Molecules Do the Work. *Top. Catal.* **2015**, *58*, 30−45. (f) Takeda, H.; Cometto, C.; Ishitani, O.; Robert, M. Electrons, Photons, Protons, and Earth-Abundant Metal Complexes for Molecular Catalysis of CO_2 Reduction. *ACS Catal.* **2017**, *7*, 70−88.

(6) Chen, Z.; Chen, C.; Weinberg, D. R.; Kang, P.; Concepcion, J. J.; Harrison, D. P.; Brookhart, M. S.; Meyer, T. J. Electrocatalytic reduction of CO_2 to CO by polypyridyl ruthenium complexes. *Chem. Commun.* **2011**, *47*, 12607−12609.

(7) Thoi, V. S.; Kornienko, N.; Margarit, C. G.; Yang, P.; Chang, C. J. Visible-light photoredox catalysis: Selective reduction of carbon dioxide to carbon monoxide by a nickel *N*-heterocyclic carbene-isoquinoline complex. *J. Am. Chem. Soc.* **2013**, *135*, 14413−14424.

(8) Agarwal, J.; Shaw, T. W.; Stanton, C. J., III; Majetich, G. F.; Bocarsly, A. B.; Schaefer, H. F., III NHC-containing manganese(I) electrocatalysts for the two-electron reduction of CO_2. *Angew. Chem., Int. Ed.* **2014**, *53*, 5152−5155.

(9) Sheng, M.; Jiang, N.; Gustafson, S.; You, B.; Ess, D. H.; Sun, Y. A nickel complex with a biscarbene pincer-type ligand shows high electrocatalytic reduction of CO_2 over H_2O. *Dalton Trans.* **2015**, *44*, 16247−16250.

(10) Franco, F.; Pinto, M. F.; Royo, B.; Lloret-Fillol, J. A highly active *N*-heterocyclic carbene manganese(I) complex for selective electrocatalytic CO_2 reduction to CO. *Angew. Chem., Int. Ed.* **2018**, *57*, 4603−4606.

(11) Myren, T. H. T.; Lilio, A. M.; Huntzinger, C. G.; Horstman, J. W.; Stinson, T. A.; Donadt, T. B.; Moore, C.; Lama, B.; Funke, H. H.; Luca, O. R. Manganese *N*-heterocyclic carbene pincers for the electrocatalytic reduction of carbon dioxide. *Organometallics* **2019**, *38*, 1248−1253.

(12) Liyanage, N. P.; Dulaney, H. A.; Huckaba, A. J.; Jurss, J. W.; Delcamp, J. H. Electrocatalytic reduction of CO_2 to CO with Re-pyridyl-NHCs: Proton source influence on rates and product selectivities. *Inorg. Chem.* **2016**, *55*, 6085−6094.
(13) Das, S.; Rodrigues, R. R.; Lamb, R. W.; Qu, F.; Reinheimer, E.; Boudreaux, C. M.; Webster, C. E.; Delcamp, J. H.; Papish, E. T. Highly active ruthenium CNC pincer photocatalysts for visible-light-driven carbon dioxide reduction. *Inorg. Chem.* **2019**, *58*, 8012−8020.
(14) Hermann, W. A. *N*-heterocyclic carbenes: A new concept in organometallic catalysis. *Angew. Chem., Int. Ed.* **2002**, *41*, 1290−1309.
(15) Nelson, D. J.; Nolan, S. P. Quantifying and understanding the electronic properties of *N*-heterocyclic carbenes. *Chem. Soc. Rev.* **2013**, *42*, 6723−6753.
(16) Hopkinson, M. N.; Richter, C.; Schedler, M.; Glorius, F. An overview of *N*-heterocyclic carbenes. *Nature* **2014**, *510*, 485−496.
(17) Huynh, H. V. Electronic properties of *N*-heterocyclic carbenes and their experimental determination. *Chem. Rev.* **2018**, *118*, 9457−9492.
(18) Su, X.; McCardle, K. M.; Panetier, J. A.; Jurss, J. W. Electrocatalytic CO_2 Reduction with Nickel Complexes Supported by Tunable Bipyridyl-*N*-Heterocyclic Carbene Donors: Understanding Redox-Active Macrocycles. *Chem. Commun.* **2018**, *54*, 3351−3354.
(19) Su, X.; McCardle, K. M.; Chen, L.; Panetier, J. A.; Jurss, J. W. Robust and Selective Cobalt Catalysts Bearing Redox-Active Bipyridyl-*N*-Heterocyclic Frameworks for Electrochemical CO_2 Reduction in Aqueous Solutions. *ACS Catal.* **2019**, *9*, 7398−7408.
(20) Shirley, H.; Su, X.; Sanjanwala, H.; Talukdar, K.; Jurss, J. W.; Delcamp, J. H. Durable Solar Powered Systems with Ni-Catalysts for Conversion of CO_2 or CO to CH_4. *J. Am. Chem. Soc.* **2019**, *141*, 6617−6622.
(21) Lacy, D. C.; McCrory, C. C. L.; Peters, J. C. Studies of Cobalt-Mediated Electrocatalytic CO_2 Reduction Using a Redox-Active Ligand. *Inorg. Chem.* **2014**, *53*, 4980−4988.
(22) White, T. A.; Maji, S.; Ott, S. Mechanistic Insights into Electrocatalytic CO_2 Reduction Within $[Ru^{II}(tpy)(NN)X]^{n+}$ Architectures. *Dalton Trans.* **2014**, *43*, 15028−15037.
(23) Chen, L.; Guo, Z.; Wei, X.-G.; Gallenkamp, C.; Bonin, J.; Anxolabéhère-Mallart, E.; Lau, K.-C.; Lau, T.-C.; Robert, M. Molecular Catalysis of the Electrochemical and Photochemical Reduction of CO_2 with Earth-Abundant Metal Complexes. Selective Production of CO vs HCOOH by Switching of the Metal Center. *J. Am. Chem. Soc.* **2015**, *137*, 10918−10921.
(24) Liu, F.-W.; Bi, J.; Sun, Y.; Luo, S.; Kang, P. Cobalt Complex with Redox-Active Imino Bipyridyl Ligand for Electrocatalytic Reduction of Carbon Dioxide to Formate. *ChemSusChem* **2018**, *11*, 1656−1663.
(25) McKinnon, M.; Ngo, K. T.; Sobottka, S.; Sarkar, B.; Ertem, M. Z.; Grills, D. C.; Rochford, J. Synergistic Metal-Ligand Redox Cooperativity for Electrocatalytic CO_2 Reduction Promoted by a Ligand-Based Redox Couple in Mn and Re Tricarbonyl Complexes. *Organometallics* **2019**, *38*, 1317−1329.
(26) Derrick, J. S.; Loipersberger, M.; Chatterjee, R.; Iovan, D. A.; Smith, P. T.; Chakarawet, K.; Yano, J.; Long, J. R.; Head-Gordon, M.; Chang, C. J. Metal-Ligand Cooperativity via Exchange Coupling Promotes Iron-Catalyzed Electrochemical CO_2 Reduction at Low Overpotentials. *J. Am. Chem. Soc.* **2020**, *142*, 20489−20501.
(27) Loipersberger, M.; Cabral, D. G. A.; Chu, D. B. K.; Head-Gordon, M. Mechanistic Insights into Co and Fe Quaterpyridine-Based CO_2 Reduction Catalysts: Metal-Ligand Orbital Interaction as the Key Driving Force for Distinct Pathways. *J. Am. Chem. Soc.* **2021**, *143*, 744−763.
(28) Xiao, Y.; Xie, F.; Zhang, H.-T.; Zhang, M.-T. Bioinspired Binickel Catalyst for Carbon Dioxide Reduction: The Importance of Metal-Ligand Cooperation. *JACS Au* **2024**, *4*, 1207−1218.
(29) Rigaku Oxford Diffraction. *CrysAlisPro Software System*, Version 1.171.41.27a; Rigaku Corporation: Oxford, UK, 2009.
(30) SCALE3 ABSPACK. *A Rigaku Oxford Diffraction Program (1.0.11,Gui:1.0.7)*, Rigaku Oxford Diffraction.
(31) Sheldrick, G. M. Crystal Structure Refinement with SHELXL. *Acta Crystallogr., Sect. C: Struct. Chem.* **2015**, *71* (1), 3−8.
(32) Sheldrick, G. M. SHELXT − Integrated Space-Group and Crystal-Structure Determination. *Acta Crystallogr., Sect. A: Found. Adv.* **2015**, *71* (1), 3−8.
(33) Dolomanov, O. V.; Bourhis, L. J.; Gildea, R. J.; Howard, J. A. K.; Puschmann, H. OLEX2: A Complete Structure Solution, Refinement and Analysis Program. *J. Appl. Crystallogr.* **2009**, *42* (2), 339−341.
(34) Frisch, M. J.; Trucks, G. W.; Schlegel, H. B.; Scuseria, G. E.; Robb, M. A.; Cheeseman, J. R.; Scalmani, G.; Barone, V.; Mennucci, B.; Petersson, G. A.; Nakatsuji, H.; Caricato, M.; Li, X.; Hratchian, H. P.; Izmaylov, A. F.; Bloino, J.; Zheng, G.; Sonnenberg, J. L.; Hada, M.; Ehara, M.; Toyota, K.; Fukuda, R.; Hasegawa, J.; Ishida, M.; Nakajima, T.; Honda, Y.; Kitao, O.; Nakai, H.; Vreven, T.; Montgomery, J. A., Jr.; Peralta, J. E.; Ogliaro, F.; Bearpark, M.; Heyd, J. J.; Brothers, E.; Kudin, K. N.; Staroverov, V. N.; Kobayashi, R.; Normand, J.; Raghavachari, K.; Rendell, A.; Burant, J. C.; Iyengar, S. S.; Tomasi, J.; Cossi, M.; Rega, N.; Millam, J. M.; Klene, M.; Knox, J. E.; Cross, J. B.; Bakken, V.; Adamo, C.; Jaramillo, J.; Gomperts, R.; Stratmann, R. E.; Yazyev, O.; Austin, A. J.; Cammi, R.; Pomelli, C.; Ochterski, J. W.; Martin, R. L.; Morokuma, K.; Zakrzewski, V. G.; Voth, G. A.; Salvador, P.; Dannenberg, J. J.; Dapprich, S.; Daniels, A. D.; Farkas, Ö.; Foresman, J. B.; Ortiz, J. V.; Cioslowski, J.; Fox, D. J. *Gaussian 09*, Revision 01,E; Gaussian, Inc.: Wallingford CT, 2009.
(35) Frisch, M. J.; Trucks, G. W.; Schlegel, H. B.; Scuseria, G. E.; Robb, M. A.; Cheeseman, J. R.; Scalmani, G.; Barone, V.; Petersson, G. A.; Nakatsuji, H.; Li, X.; Caricato, M.; Marenich, A. V.; Bloino, J.; Janesko, B. G.; Gomperts, R.; Mennucci, B.; Hratchian, H. P.; Ortiz, J. V.; Izmaylov, A. F.; Sonnenberg, J. L.; Williams-Young, D.; Ding, F.; Lipparini, F.; Egidi, F.; Goings, J.; Peng, B.; Petrone, A.; Henderson, T.; Ranasinghe, D.; Zakrzewski, V. G.; Gao, J.; Rega, N.; Zheng, G.; Liang, W.; Hada, M.; Ehara, M.; Toyota, K.; Fukuda, R.; Hasegawa, J.; Ishida, M.; Nakajima, T.; Honda, Y.; Kitao, O.; Nakai, H.; Vreven, T.; Throssell, K.; Montgomery, J. A., Jr.; Peralta, J. E.; Ogliaro, F.; Bearpark, M. J.; Heyd, J. J.; Brothers, E. N.; Kudin, K. N.; Staroverov, V. N.; Keith, T. A.; Kobayashi, R.; Normand, J.; Raghavachari, K.; Rendell, A. P.; Burant, J. C.; Iyengar, S. S.; Tomasi, J.; Cossi, M.; Millam, J. M.; Klene, M.; Adamo, C.; Cammi, R.; Ochterski, J. W.; Martin, R. L.; Morokuma, K.; Ferkas, Ö.; Foresman, J. B.; Fox, D. J. *Gaussian 16*, Revision 03,A; Gaussian, Inc.: Wallingford CT, 2016.
(36) Chai, J.-D.; Head-Gordon, M. Long-range corrected hybrid density functionals with damped atom-atom dispersion corrections. *Phys. Chem. Chem. Phys.* **2008**, *10*, 6615−6620.
(37) Marenich, A. V.; Cramer, C. J.; Truhlar, D. G. Universal solvation model based on solute electron density and on a continuum model of the solvent defined by the bulk dielectric constant and atomic surface tensions. *J. Phys. Chem. B* **2009**, *113*, 6378−6396.
(38) Weigend, F.; Ahlrichs, R. Balanced basis sets of split valence, triple zeta valence and quadruple zeta valence quality for H to Rn: Design and assessment of accuracy. *Phys. Chem. Chem. Phys.* **2005**, *7*, 3297−3305.
(39) Weigend, F. Accurate Coulomb-fitting basis sets for H to Rn. *Phys. Chem. Chem. Phys.* **2006**, *8*, 1057−1065.
(40) Gonzalez, C.; Schlegel, H. B. An improved algorithm for reaction path following. *J. Chem. Phys.* **1989**, *90*, 2154−2161.
(41) Gonzalez, C.; Schlegel, H. B. Reaction path following in mass-weighted internal coordinates. *J. Chem. Phys.* **1990**, *94*, 5523−5527.
(42) Thom, A. J. W.; Sundstrom, E. J.; Head-Gordon, M. LOBA: a localized orbital bonding analysis to calculate oxidation states, with application to a model water oxidation catalyst. *Phys. Chem. Chem. Phys.* **2009**, *11*, 11297−11304.
(43) Shao, Y.; Gan, Z.; Epifanovsky, E.; Gilbert, A. T. B.; Wormit, M.; Kussmann, J.; Lange, A. W.; Behn, A.; Deng, J.; Feng, X.; Ghosh, D.; Goldey, M.; Horn, P. R.; Jacobson, L. D.; Kaliman, I.; Khaliullin, R. Z.; Kuś, T.; Landau, A.; Liu, J.; Proynov, E. I.; Rhee, Y. M.; Richard, R. M.; Rohrdanz, M. A.; Steele, R. P.; Sundstrom, E. J.; Woodcock, H. L.; Zimmerman, P. M.; Zuev, D.; Albrecht, B.; Alguire, E.; Austin, B.; Beran, G. J. O.; Bernard, Y. A.; Berquist, E.; Brandhorst,

https://doi.org/10.1021/acsomega.4c02520
ACS Omega 2024, 9, 34555−34566

K.; Bravaya, K. B.; Brown, S. T.; Casanova, D.; Chang, C.-M.; Chen, Y.; Chien, S. H.; Closser, K. D.; Crittenden, D. L.; Diedenhofen, M.; DiStasio, R. A.; Do, H.; Dutoi, A. D.; Edgar, R. G.; Fatehi, S.; Fusti-Molnar, L.; Ghysels, A.; Golubeva-Zadorozhnaya, A.; Gomes, J.; Hanson-Heine, M. W. D.; Harbach, P. H. P.; Hauser, A. W.; Hohenstein, E. G.; Holden, Z. C.; Jagau, T.-C.; Ji, H.; Kaduk, B.; Khistyaev, K.; Kim, J.; Kim, J.; King, R. A.; Klunzinger, P.; Kosenkov, D.; Kowalczyk, T.; Krauter, C. M.; Lao, K. U.; Laurent, A. D.; Lawler, K. V.; Levchenko, S. V.; Lin, C. Y.; Liu, F.; Livshits, E.; Lochan, R. C.; Luenser, A.; Manohar, P.; Manzer, S. F.; Mao, S.-P.; Mardirossian, N.; Marenich, A. V.; Maurer, S. A.; Mayhall, N. J.; Neuscamman, E.; Oana, C. M.; Olivares-Amaya, R.; O'Neill, D. P.; Parkhill, J. A.; Perrine, T. M.; Peverati, R.; Prociuk, A.; Rehn, D. R.; Rosta, E.; Russ, N. J.; Sharada, S. M.; Sharma, S.; Small, D. W.; Sodt, A.; Stein, T.; Stück, D.; Su, Y.-C.; Thom, A. J. W.; Tsuchimochi, T.; Vanovschi, V.; Vogt, L.; Vydrov, O.; Wang, T.; Watson, M. A.; Wenzel, J.; White, A.; Williams, C. F.; Yang, J.; Yeganeh, S.; Yost, S. R.; You, Z.-Q.; Zhang, I. Y.; Zhang, X.; Zhao, Y.; Brooks, B. R.; Chan, G. K. L.; Chipman, D. M.; Cramer, C. J.; Goddard, W. A.; Gordon, M. S.; Hehre, W. J.; Klamt, A.; Schaefer, H. F.; Schmidt, M. W.; Sherrill, C. D.; Truhlar, D. G.; Warshel, A.; Xu, X.; Aspuru-Guzik, A.; Baer, R.; Bell, A. T.; Besley, N. A.; Chai, J.-D.; Dreuw, A.; Dunietz, B. D.; Furlani, T. R.; Gwaltney, S. R.; Hsu, C.-P.; Jung, Y.; Kong, J.; Lambrecht, D. S.; Liang, W.; Ochsenfeld, C.; Rassolov, V. A.; Slipchenko, L. V.; Subotnik, J. E.; Van Voorhis, T.; Herbert, J. M.; Krylov, A. I.; Gill, P. M. W.; Head-Gordon, M. Advances in molecular quantum chemistry contained in the Q-Chem 4 program package. *Mol. Phys.* **2015**, *113*, 184−215.

(44) Grimme, S. Supramolecular binding thermodynamics by dispersion-corrected density functional theory. *Chem. - Eur. J.* **2012**, *18*, 9955−9964.

(45) Li, Y.-P.; Gomes, J.; Sharada, S. M.; Bell, A. T.; Head-Gordon, M. Improved Force-Field Parameters for QM/MM Simulations of the Energies of Adsorption for Molecules in Zeolites and a Free Rotor Correction to the Rigid Rotor Harmonic Oscillator Model for Adsorption Enthalpies. *J. Phys. Chem. C* **2015**, *119*, 1840−1850.

(46) Marenich, A. V.; Ho, J.; Coote, M. L.; Cramer, C. J.; Truhlar, D. G. Computational Electrochemistry: prediction of liquid-phase reduction potentials. *Phys. Chem. Chem. Phys.* **2014**, *16*, 15068−15106.

(47) Bondi, A. van der Waals Volumes and Radii. *J. Phys. Chem. A* **1964**, *68*, 441−451.

(48) Cordero, B.; Gómez, V.; Platero-Prats, A. E.; Revés, M.; Echeverría, J.; Cremades, E.; Barragán, F.; Alvarez, S. Covalent radii revisited. *Dalton Trans.* **2008**, 2832−2838.

(49) Li, C. W.; Kanan, M. W. CO_2 reduction at low overpotential on Cu electrodes resulting from the reduction of thick Cu_2O films. *J. Am. Chem. Soc.* **2012**, *134*, 7231−7234.

(50) Roberts, F. S.; Kuhl, K. P.; Nilsson, A. High selectivity for ethylene from carbon dioxide reduction over copper nanocube electrocatalysts. *Angew. Chem., Int. Ed.* **2015**, *54*, 5179−5182.

(51) Chen, C. S.; Handoko, A. D.; Wan, J. H.; Ma, L.; Ren, D.; Yeo, B. S. Stable and selective electrochemical reduction of carbon dioxide to ethylene on copper mesocrystals. *Catal. Sci. Technol.* **2015**, *5*, 161−168.

(52) Nitopi, S.; Bertheussen, E.; Scott, S. B.; Liu, X.; Engstfeld, A. K.; Horch, S.; Seger, B.; Stephens, I. E. L.; Chan, K.; Hahn, C.; Nørskov, J. K.; Jaramillo, T. F.; Chorkendorff, I. Progress and perspectives of electrochemical CO_2 reduction on copper in aqueous electrolyte. *Chem. Rev.* **2019**, *119*, 7610−7672.

(53) Zhao, J.; Xue, S.; Barber, J.; Zhou, Y.; Meng, J.; Ke, X. An overview of Cu-based heterogeneous electrocatalysts for CO_2 reduction. *J. Mater. Chem. A* **2020**, *8*, 4700−4734.

(54) Sullivan, B. P.; Bolinger, C. M.; Conrad, D.; Vining, W. J.; Meyer, T. J. One- and two-electron pathways in the electrocatalytic reduction of CO_2 by *fac*-Re(bpy)$(CO)_3$Cl (bpy = 2,2′-bipyridine). *J. Chem. Soc., Chem. Commun.* **1985**, 1414−1416.

(55) (a) Bolinger, C. M.; Sullivan, B. P.; Conrad, D.; Gilbert, J. A.; Story, N.; Meyer, T. J. Electrocatalytic reduction of CO_2 based on polypyridyl complexes of rhodium and ruthenium. *J. Chem. Soc., Chem. Commun.* **1985**, 796−797. (b) Bolinger, C. M.; Story, N.; Sullivan, B. P.; Meyer, T. J. Electrocatalytic reduction of carbon dioxide by 2,2'-bipyridine complexes of rhodium and iridium. *Inorg. Chem.* **1988**, *27*, 4582−4587.

(56) Xiao, L.; Johnson, K. E. Electrochemistry of 1-butyl-3-methyl-1*H*-imidazolium tetrafluoroborate ionic liquid. *J. Electrochem. Soc.* **2003**, *150* (6), E307−E311.

(57) Gorodetsky, B.; Ramnial, T.; Branda, N. R.; Clyburne, J. A. C. Electrochemical reduction of an imidazolium cation: a convenient preparation of imidazole-2-ylidenes and their observation in an ionic liquid. *Chem. Commun.* **2004**, 1972−1973.

(58) Orsini, M.; Chiarotto, I.; Elinson, M. N.; Sotgiu, G.; Inesi, A. Benzoin condensation in 1,3-dialkylimidazolium ionic liquids via electrochemical generation of *N*-heterocyclic carbene. *Electrochem. Commun.* **2009**, *11*, 1013−1017.

(59) Feroci, M.; Chiarotto, I.; Orsini, M.; Pelagalli, R.; Inesi, A. Umpolung reactions in an ionic liquid catalyzed by electrogenerated *N*-heterocyclic carbenes. Synthesis of saturated esters from activated *α,β*-unsaturated aldehydes. *Chem. Commun.* **2012**, *48*, 5361−5363.

(60) Feroci, M.; Chiarotto, I.; Ciprioti, S. V.; Inesi, A. On the reactivity and stability of electrogenerated *N*-heterocyclic carbene in parent 1-butyl-3-methyl-1*H*-imidazolium tetrafluoroborate: formation and use of *N*-heterocyclic carbene-CO_2 adduct as latent catalyst. *Electrochim. Acta* **2013**, *109*, 95−101.

(61) Gokturk, P. A.; Donmez, S. E.; Ulgut, B.; Türkmen, Y. E.; Suzer, S. Optical and XPS evidence for the electrochemical generation of an *N*-heterocyclic carbene and its CS_2 adduct from the ionic liquid [bmim][PF_6]. *New J. Chem.* **2017**, *41*, 10299−10304.

(62) Rocco, D.; Chiarotto, I.; D'Anna, F.; Mattiello, L.; Pandolfi, F.; Rizzo, C.; Feroci, M. Cathodic behavior of dicationic imidazolium bromides: the role of the spacer. *ChemElectroChem* **2019**, *6*, 4275−4283.

(63) Angamuthu, R.; Byers, P.; Lutz, M.; Spek, A. L.; Bouwman, E. Electrocatalytic CO_2 conversion to oxalate by a copper complex. *Science* **2010**, *327*, 313−315.

(64) Pokharel, U. R.; Fronczek, F. R.; Maverick, A. W. Reduction of carbon dioxide to oxalate by a binuclear copper complex. *Nat. Commun.* **2014**, *5*, No. 5883.

(65) Cook, B. J.; Di Francesco, G. N.; Abboud, K. A.; Murray, L. J. Countercations and solvent influence CO_2 reduction to oxalate by chalogen-bridged tricopper cyclophanates. *J. Am. Chem. Soc.* **2018**, *140*, 5696−5700.

(66) Saha, S.; Sahil, S. T.; Mazumder, M. M. R.; Stephens, A. M.; Cronin, B.; Duin, E. C.; Jurss, J. W.; Farnum, B. H. Synthesis, Characterization, and Electrocatalytic Activity of Bis(pyridylimino)-Isoindoline Cu(II) and Ni(II) Complexes. *Dalton Trans.* **2021**, *50*, 926−935.

(67) Dietrich-Buchecker, C. O.; Sauvage, J.-P.; Kern, J. M. Templated synthesis of interlocked macrocyclic ligands: The catenands. *J. Am. Chem. Soc.* **1984**, *106*, 3043−3045.

(68) Cowan, J. A.; Sanders, J. K. M. Reductive demetallation of porphyrins: Evidence for peripheral and axial modes of reduction. *Tetrahedron Lett.* **1986**, *27*, 1201−1204.

(69) Kumar, M.; Neta, P.; Sutter, T. P. G.; Hambright, P. One-electron reduction and demetallation of copper porphyrins. *J. Phys. Chem. A* **1992**, *96*, 9571−9575.

(70) Scott, S. M.; Gordon, K. C.; Burrell, A. K. Spectroelectrochemical studies of copper(I) complexes with binaphthyridine and biquinoline ligands. Crystal structure determination of bis(6,7-dihydrodipyrido[2,3-b:3′,2′-j][1,10]phenanthroline)copper(I) tetrafluoroborate. *Inorg. Chem.* **1996**, *35*, 2452−2457.

(71) Woodin, K. S.; Heroux, K. J.; Boswell, C. A.; Wong, E. H.; Weisman, G. R.; Niu, W.; Tomellini, S. A.; Anderson, C. J.; Zakharov, L. N.; Rheingold, A. L. Kinetic inertness and electrochemical behavior of copper(II) tetraazamacrocyclic complexes: Possible implications for in vivo stability. *Eur. J. Inorg. Chem.* **2005**, *2005*, 4829−4833.

(72) Roznyatovskaya, N. V.; Vassiliev, S. Y.; Yusipovich, A. I.; Tsirlina, G. A.; Roznyatovskii, V. V. Aqueous electrochemistry of binuclear copper complex with Robson-type ligand: dissolved versus

https://doi.org/10.1021/acsomega.4c02520
ACS Omega 2024, 9, 34555−34566

surface-immobilized reactant. *J. Solid State Electrochem.* **2005**, *9*, 581−589.
(73) Ngo, T. H.; Rossom, W. V.; Dehaen, W.; Maes, W. Reductive demetallation of Cu-corroles − a new protective strategy towards functional free-base corroles. *Org. Biomol. Chem.* **2009**, *7*, 439−443.
(74) Lima, L. M. P.; Esteban-Gómez, D.; Delgado, R.; Platas-Iglesias, C.; Tripier, R. Monopicolinate cyclen and cyclam derivatives for stable copper(II) complexation. *Inorg. Chem.* **2012**, *51*, 6916−6927.
(75) Dash, C.; Das, A.; Yousufuddin, M.; Dias, H. V. R. Isolable, Copper(I) Dicarbonyl Complexes Supported by *N*-Heterocyclic Carbenes. *Inorg. Chem.* **2013**, *52*, 1584−1590.
(76) Kuehn, L.; Eichhorn, A. F.; Marder, T. B.; Radius, U. Copper(I) Complexes of *N*-Alkyl-Substituted *N*-Heterocyclic Carbenes. *J. Organomet. Chem.* **2019**, *881*, 25−33.
(77) Almallah, H.; Brenner, E.; Matt, D.; Gourlaouen, C.; Hissler, M. Stereochemical Control of Tricoordinate Copper(I) Complexes Based on *N*-(9-Alkyl-9-fluorenyl)-Substituted Heterocyclic Carbenes. *Synthesis* **2021**, *53*, 1785−1794.
(78) Bezuidenhout, D. I.; Kleinhans, G.; Guisado-Barrios, G.; Liles, D. C.; Ung, G.; Bertrand, G. Isolation of a Potassium Bis(1,2,3-triazol-5-ylidene)carbazolide: A Stabilizing Pincer Ligand for Reactive Late Transition Metal Complexes. *Chem. Commun.* **2014**, *50*, 2431−2433.
(79) Ghavami, Z. S.; Anneser, M. R.; Kaiser, F.; Altmann, P. J.; Hofmann, B. J.; Schlagintweit, J. F.; Grivani, G.; Kühn, F. E. A Bench Stable Formal Cu(III) *N*-Heterocyclic Carbene Accessible from Simple Copper(II) Acetate. *Chem. Sci.* **2018**, *9*, 8307−8314.
(80) Liu, Y.; Resch, S. G.; Klawitter, I.; Cutsail, G. E., III; Demeshko, S.; Dechert, S.; Kühn, F. E.; DeBeer, S.; Meyer, F. An Adaptable *N*-Heterocyclic Carbene Macrocycle Hosting Copper in Three Oxidation States. *Angew. Chem., Int. Ed.* **2020**, *59*, 5696−5705.
(81) Kuhn, N.; Steimann, M.; Weyers, G. Synthesis and properties of 1,3-diisopropyl-4,5-dimethylimidazolium-2-carboxylate. A stable carbene adduct of carbon dioxide. *Z. Naturforsch., B* **1999**, *54b*, 427−433.
(82) Duong, H. A.; Tekavec, T. N.; Arif, A. M.; Louie, J. Reversible carboxylation of *N*-heterocyclic carbenes. *Chem. Commun.* **2004**, 112−113.
(83) Tommasi, I.; Sorrentino, F. Utilisation of 1,3-dialkylimidazolium-2-carboxylates as CO_2-carriers in the presence of Na^+ and K^+: application in the synthesis of carboxylates, monomethylcarbonate anions and halogen-free ionic liquids. *Tetrahedron Lett.* **2005**, *46*, 2141−2145.
(84) Tudose, A.; Demonceau, A.; Delaude, L. Imidazol(in)ium-2-carboxylates as *N*-heterocyclic carbene precursors in ruthenium-arene catalysts for olefin metathesis and cyclopropanation. *J. Organomet. Chem.* **2006**, *691*, 5356−5365.
(85) Schössler, W.; Regitz, M. Stabile dipole asu 1,1′,3,3′-tetraphenyl-2,2′-biimidazolidinyliden und acyliso- bzw. Acylisothiocyanaten. *Chem. Ber.* **1974**, *107*, 1931−1948.
(86) Holbrey, J. D.; Reichert, W. M.; Tkatchenko, I.; Bouajila, E.; Walter, O.; Tommasi, I.; Rogers, R. D. 1,3-Dimethylimidazolium-2-carboxylate: the unexpected synthesis of an ionic liquid precursor and carbene-CO_2 adduct. *Chem. Commun.* **2003**, 28−29.
(87) Tommasi, I.; Sorrentino, F. Synthesis of 1,3-dialkylimidazolium-2-carboxylates by direct carboxylation of 1,3-dialkylimidazolium chlorides with CO_2. *Tetrahedron Lett.* **2006**, *47*, 6453−6456.
(88) Riduan, S. N.; Zhang, Y.; Ying, J. Y. Conversion of carbon dioxide into methanol with silanes over *N*-heterocyclic carbene catalysts. *Angew. Chem., Int. Ed.* **2009**, *48*, 3322−3325.
(89) Luca, O. R.; McCrory, C. C. L.; Dalleska, N. F.; Koval, C. A. The selective electrochemical conversion of preactivated CO_2 to methane. *J. Electrochem. Soc.* **2015**, *162*, H473−H476.
(90) Voutchkova, A. M.; Appelhans, L. N.; Chianese, A. R.; Crabtree, R. H. Disubstituted imidazolium-2-carboxylates as efficient precursors to *N*-heterocyclic carbene complexes of Rh, Ru, Ir, and Pd. *J. Am. Chem. Soc.* **2005**, *127*, 17624−17625.
(91) Voutchkova, A. M.; Feliz, M.; Clot, E.; Eisenstein, O.; Crabtree, R. H. Imidazolium carboxylates as versatile and selective *N*-heterocyclic carbene transfer agents: Synthesis, mechanism, and applications. *J. Am. Chem. Soc.* **2007**, *129*, 12834−12846.

https://doi.org/10.1021/acsomega.4c02520
ACS Omega 2024, 9, 34555−34566